

Antitrypanosomal Lead Discovery: Identification of a Ligand-Efficient Inhibitor of *Trypanosoma cruzi* CYP51 and Parasite Growth

Grasiella Andriani,[§] Emanuele Amata,[†] Joel Beatty,[†] Zeke Clements,[†] Brian J. Coffey,[†] Gilles Courtemanche,[#] William Devine,[†] Jessey Erath,[§] Cristin E. Juda,[†] Zdzislaw Wawrzak,[⊥] JodiAnne T. Wood,[‡] Galina I. Lepesheva,^{*,||} Ana Rodriguez,^{*,§} and Michael P. Pollastri^{*,†,‡}

[†]Department of Chemistry and Chemical Biology, and [‡]Center for Drug Discovery, Northeastern University, Boston, Massachusetts 02115, United States

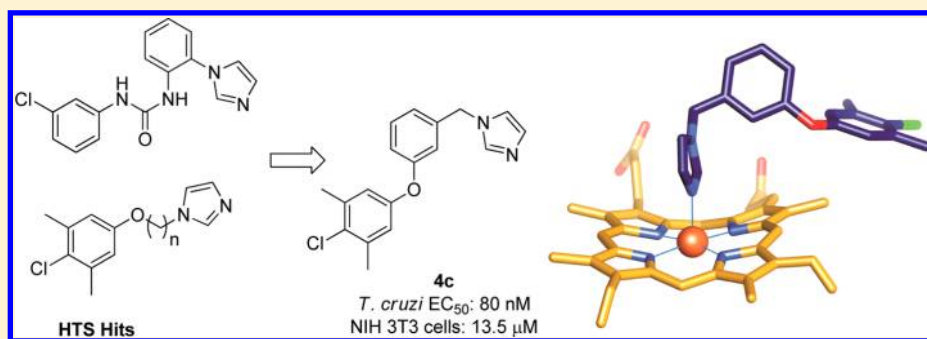
[§]Division of Parasitology, Department of Microbiology, New York University School of Medicine, New York, New York 10010, United States

^{||}Department of Biochemistry School of Medicine, Institute for Global Health, Vanderbilt University School of Medicine, Nashville, Tennessee 37232, United States

[⊥]Synchrotron Research Center, Life Science Collaborative Access Team, Northwestern University, Argonne, Illinois 60439, United States

[#]Sanofi Research, 195 Route d'Espagne BP13669, 31036 Toulouse Cedex1, France

S Supporting Information



ABSTRACT: Chagas disease is caused by the intracellular protozoan parasite *Trypanosoma cruzi*, and current drugs are lacking in terms of desired safety and efficacy profiles. Following on a recently reported high-throughput screening campaign, we have explored initial structure–activity relationships around a class of imidazole-based compounds. This profiling has uncovered compounds **4c** (NEU321) and **4j** (NEU704), which are potent against in vitro cultures of *T. cruzi* and are greater than 160-fold selective over host cells. We report in vitro drug metabolism and properties profiling of **4c** and show that this chemotype inhibits the *T. cruzi* CYP51 enzyme, an observation confirmed by X-ray crystallographic analysis. We compare the binding orientation of **4c** to that of other, previously reported inhibitors. We show that **4c** displays a significantly better ligand efficiency and a shorter synthetic route over previously disclosed CYP51 inhibitors, and should therefore be considered a promising lead compound for further optimization.

INTRODUCTION

In Latin America, an estimated 10 million people are infected with *Trypanosoma cruzi*, the causative parasite for Chagas disease. This rate of infection results in over 10 000 deaths per year, primarily due to the cardiomyopathy end point that is the most typical pathology resulting from chronic *T. cruzi* infection. Current drugs, such as benznidazole and nifurtimox, are fairly effective when utilized during the acute stage of the disease, yet success in curing chronic Chagas disease has been limited. Moreover, these drugs have toxicity limitations. Despite these limitations and the 25 million people at risk, the pipeline for new drugs is lacking, primarily due to the lack of financial incentives for undertaking the expensive process of drug

discovery for a condition such as Chagas disease, which predominantly affects a very poor population. Nonetheless, due to immigration into North America and Europe from Latin America, an increasing burden of disease is becoming apparent.¹

Academic drug discovery has made significant inroads toward filling the gap for new therapeutics. Repurposed antifungal agents, such as the approved drug posaconazole,² the investigational compound E1224 (a ravuconazole prodrug), and Tak-187,³ have been assessed in clinical trials for Chagas

Received: January 3, 2013

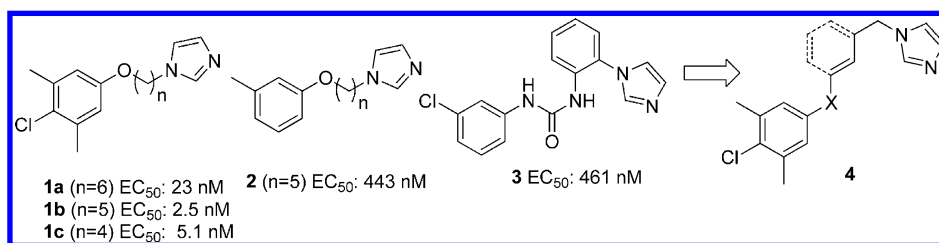


Figure 1. Anti-*T. cruzi* compounds previously discovered via HTS approaches, leading to the design principle 4.

disease. Other research groups have expanded a class of farnesyl transferase inhibitors (such as tipifarnib) to improve safety and efficacy;^{4,5} the mechanism of action of all of these compounds is via the sterol biosynthesis pathway, inhibiting cytochrome P450 sterol 14 α -demethylase (*T. cruzi* CYP51).^{6,7}

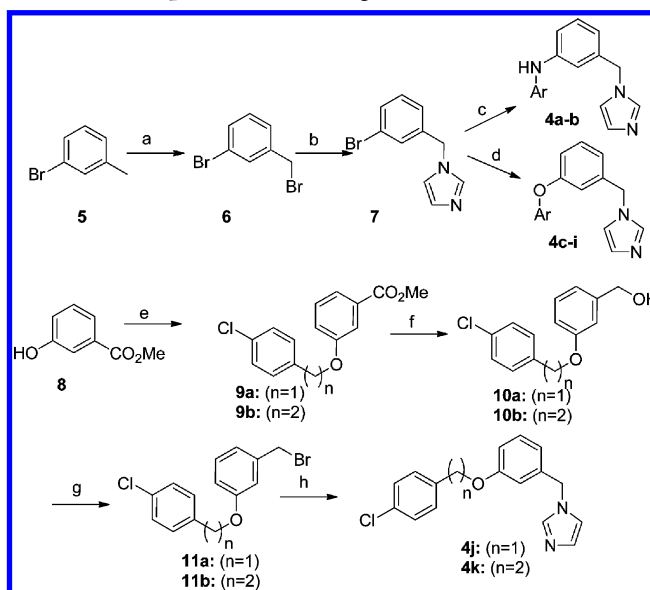
High-throughput screening (HTS) approaches have begun to reveal new compounds with anti-*T. cruzi* activity. One such screening campaign has resulted in compounds that show *in vivo* activity.⁸ We evaluated the screening hits from the HTS campaign (303 286 compounds) in the context of those identified in a previous report⁹ and highlight in Figure 1 a promising class of imidazole-based inhibitors that effectively inhibit infection of mammalian host cells by *T. cruzi* trypomastigotes. In particular, compounds 1, 2, and related analogs were identified in the HTS. A third imidazole-bearing class, typified by 3, showed activity approximately equal to that of 2. A related set of compounds was recently reported in a separate HTS that probed *T. cruzi* CYP51 in a biochemical assay.¹⁰ Taken together, these compounds present a general structural motif consisting of an imidazole ring that is connected to a lipophilic tail via a linker of variable length and flexibility. We therefore looked to optimize this chemotype with an eye toward improving potency against *T. cruzi* while maintaining the low level of host cell toxicity observed in the HTS. Further, several of the compounds of interest feature long hydrocarbon linkers, which are implicated in poor bioavailability and metabolic properties.¹¹

RESULTS

Medicinal Chemistry. With these goals in mind, we first sought to replace the alkyl chain linker with a scaffold that would appropriately present the proposed pharmacophoric elements. This was pursued by the synthesis of ring-constrained analogs, typified by structure 4 (Figure 1), which represents an analog of the potent HTS hit 1c. To that end, benzylic bromination of 3-bromotoluene followed by nucleophilic displacement with imidazole provided 7 (Scheme 1). This was subjected to Buchwald–Hartwig coupling to give diaryl amines 4a–b or Ullman coupling to give diaryl ethers 4c–i. Compounds 4j–k were constructed from methyl 3-hydroxybenzoate via a sequence of Ullman coupling and conversion of the methyl ester to a benzyl bromide, which was substrate for alkylation of imidazole.

The screening results of this initial SAR exploration are shown in Table 1. Activity against *T. cruzi* was determined in a mammalian host cell infection assay measuring *T. cruzi* trypomastigote infection during 96 h, counterscreened against uninfected host cells (NIH 3T3 cells). Gratifyingly, the ring-constrained analog 4c (NEU321), directly designed from 1c, was quite potent (80 nM). Compound 4a was approximately equipotent to 4c, and all of the analogs tested were at least 60-fold selective over host cells. Substitution with lipophilic groups

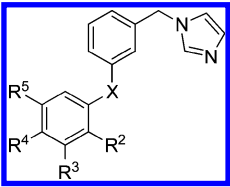
Scheme 1. Preparation of Analogs 4a–e^a



^aReagents and conditions: (a) *N*-bromosuccinimide, CH_2Cl_2 ; (b) imidazole, DMF, MW 180 °C, 10 min; (c) H_2N-Ar , $Pd_2(dba)_3$, DPEPhos, DMF, MW 170 °C, 20 min; (d) CuI , $HO-Ar$, Cs_2CO_3 , $Me_2NCH_2CO_2H$; (e) 4-chlorobenzyl bromide or 1-(2-bromoethyl)-4-chlorobenzene, K_2CO_3 , DMF, 60 °C, 1 h; (f) $LiAlH_4$, THF; (g) *N*-bromosuccinimide, PPh_3 ; and (h) imidazole, DMF, 100 °C, 1 h.

on this ring is required; a loss of ~20-fold in potency was observed by removal of all substituents (cf., 4i). Readdition of the chlorine atom improved potency by 2.5-fold (4i versus 4g), and although addition of a methyl group to 4i provided a 5-fold improvement in potency (cf., 4f), addition of a second (4e) showed no effect on *T. cruzi* cell activity. The regiochemical requirement for the aryl methyl group was explored, and the *meta*-substitution of 4f affords approximately 2X in activity over the *ortho* isomer (4h). Extending the linker length by one atom leads to doubling of potency (4j, NEU704), but further extension (4k) diminishes activity.

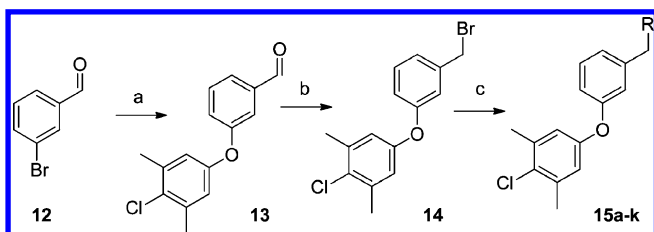
We designed a series of heterocyclic replacements for the imidazole ring to assess this region of the molecule as well. Nitrogen-linked analogs 15a–k were accessed by reaction of the benzyl bromide 14 with various nitrogen heterocycles (Scheme 2). The bromide 14 was prepared in two steps from 3-bromobenzaldehyde 12. Carbon-linked analogs 20 and 21 were prepared from the corresponding bromide 16 via a sequence of Ullmann coupling, acylhydrazide formation, and dehydrative cyclization (Scheme 3). Screening data for compounds 15, 20, and 21 are listed in Table 2, showing that the imidazole moiety of 4c is by far a more potent growth inhibitor than even isosteric heterocycles like the pyrazole 15c and triazoles 15a, b, f, and h.

Table 1. Potency of Analogs of 4 as *T. cruzi* Growth Inhibitors^a


compound	X	R ²	R ³	R ⁴	R ⁵	<i>T. cruzi</i> EC ₅₀ (μM)	NIH 3T3 EC ₅₀ (μM)	selectivity
4a	NH	CH ₃	H	NO ₂	H	0.072	>100	>1000
4b	NH	H	OCH ₃	H	H	0.167	>100	>500
4c	O	H	CH ₃	Cl	CH ₃	0.08	13.5	169
4d	O	H	Ph	H	H	0.282	34	121
4e	O	H	CH ₃	H	CH ₃	0.33	>100	>300
4f	O	H	CH ₃	H	H	0.33	78.7	238
4g	O	H	H	Cl	H	0.65	>100	>150
4h	O	CH ₃	H	H	H	0.711	79.3	112
4i	O	H	H	H	H	1.63	>100	>60
4j	OCH ₂	H	H	Cl	H	0.042	76.2	1814
4k	OCH ₂ CH ₂	H	H	Cl	H	0.53	71.1	134
benznidazole						1.9	>50	<26

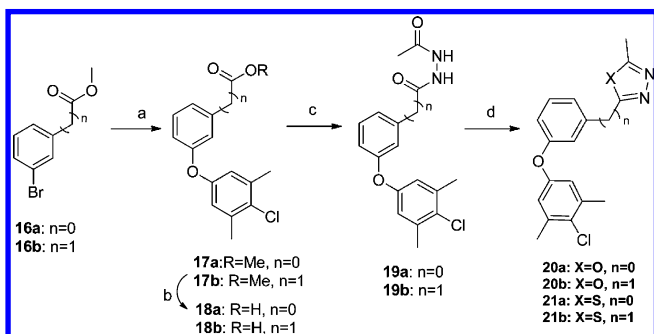
^aEC₅₀ values were determined as the average of three independent experiments performed on different days, and SEM ≤ 30%.

Scheme 2. Synthesis of Various N-Linked Imidazole Replacements 15^a



^aReagents and conditions: (a) 4-chloro-3,5-dimethylphenol, Cs₂CO₃, CuI, 2-(dimethylamino)acetic acid, 1,4-dioxane, 180 °C, 12 h; (b) TMSCl, 1,1,3,3-tetramethyldisiloxane, LiBr, CH₃CN, 80 °C, overnight; (c) heterocycle, amine or indole, K₂CO₃, DMF, 50 °C, 3 h.

Scheme 3. Synthesis of Various C-Linked Imidazole Replacements 20 and 21^a



^aReagents and conditions: (a) 4-chloro-3,5-dimethylphenol, Cs₂CO₃, CuI, 2-(dimethylamino)acetic acid, 1,4-dioxane, 180 °C, 9 h; (b) THF, LiOH, H₂O, room temperature, 2 h; (c) H₂NNHAc, HOBT, EDC, DMF, room temperature, 5 h; (d) POCl₃, 110 °C, 1 h; or Lawesson's reagent, 1,4-dioxane, 100 °C, 2 h.

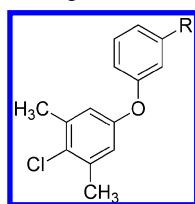
To investigate whether the effect of 4c on *T. cruzi* is reversible, the compound was washed off the cultures at different times after infection. In two distantly related strains of *T. cruzi* (Tulahuen and Y), we observed that incubation for 24 h with 4c is sufficient to inhibit *T. cruzi* replication during the

96 h of the assay, while benznidazole required 48–72 h (Figure 2).

We then evaluated the phenotypic effect of 4c on *T. cruzi* infection of host cells. We observed that 4c had a pronounced inhibitory effect on *T. cruzi* replication comparable to benznidazole, because individual parasites that were able to invade, but not replicate, are observed within host cells (Figure 3).

In Vitro Profiling of Absorption, Distribution, Metabolism, and Excretion Properties. We evaluated 4c in vitro assessments of metabolic and physicochemical properties, to ascertain parameters that required further optimization (Table 3). This compound shows good microsomal stability in human, rat, and mouse microsomes, and the percentage is only slightly reduced in the presence of quinidine (a CYP2D6 inhibitor) and ketoconazole (CYP3A4 inhibitor), indicating that metabolism of 4c is mediated in part, but not entirely, by CYP2D6 and CYP3A4. Compound 4c is also fully stable in human and mouse plasma, and is highly permeable through Caco-2 cell monolayers. However, perhaps not surprisingly, 4c is highly plasma protein bound (>99.8%), which suggests low bioavailability in vivo. Further, this compound displays strong inhibition of the hERG ion channel (94% at 10 μM); because this target is implicated in cardiotoxicity, there are significant concerns regarding this compound's safety in chronic chagasic patients that are likely to have existing cardiovascular issues due to the infection.

Mechanism of Action Hypothesis. Confident that the imidazole is key to binding, we noted that this moiety is indeed reminiscent of other inhibitors described for *T. cruzi* activity, such as tipifarnib and its analogs,¹² posaconazole,¹³ and VNF^{13,14} (Figure 4), all of which inhibit parasite growth via blockade of *T. cruzi* sterol 14α-demethylase (CYP51). This has been shown to be a central enzyme for parasitic sterol biosynthesis, the pathway essential in all life stages of *T. cruzi* that leads to formation of ergosterol and related structures from lanosterol (through eburicol as the *T. cruzi* CYP51 substrate).¹³ We hypothesized that the class of compounds typified by 4 may be inhibiting parasite growth via the same mechanism.

Table 2. Potency of Analogs 15, 20, and 21^a

Compound	R	<i>T. cruzi</i> EC ₅₀ (μM)	3T3 EC ₅₀ (μM)
15a		1.1	66.8
15b		1.1	75.9
15c		2.8	> 100
15d		3.7	>100
15e		3.7	40.0
15f		5.4	> 100
15g		6.2	29.7
15h		11.2	> 100
15i		10.7	> 100
15j		9.8	> 100
15k		13.4	> 100
20a		14.1	46.1
21a		12.3	>100
20b		3.4	6.2
21b		2.2	3.8

^aEC₅₀ values were determined as the average of three independent experiments performed on different days, and SEM ≤ 30%.

To experimentally confirm this, we tested binding of **4b**, **4c**, and **4h** to recombinant *T. cruzi* CYP51, measuring a dose-responsive type 2 spectroscopic shift that occurs upon coordination of a Lewis-basic atom of the inhibitor to the heme iron of the enzyme (Figure 5, Table 4).¹⁴ These experiments uncovered *K_d* values that correlated well with the EC₅₀ values observed in parasite cultures.

As a measure of binding energy per heavy atom of a drug compound interacting with a target, ligand efficiency (LE) is a useful metric for comparing compounds.¹⁵ LE is typically calculated by the dividing the *pK_d* or *pEC₅₀* by the number of heavy atoms in the molecule. From this standpoint, a compound that is intended to serve as a starting point for further optimization should have an LE ≥ 0.3.¹⁵ Table 4 lists

the LE values calculated for those compounds for which the *T. cruzi* CYP51 binding data were obtained, in comparison with other established inhibitors. Compounds **4b**, **4c**, and **4h** do indeed represent an attractive starting point for further optimization.

X-ray Crystallographic Analysis. X-ray crystallography has revealed the binding orientations of posaconazole and VNF complexed to *T. cruzi* CYP51, and it was noted that the inhibitors bound in the pocket in opposite orientations to each other.¹² Briefly, while the long arm of posaconazole lies inside the CYP51 substrate access channel, protruding through the channel entrance above the protein surface, the two-ring arm of VNF is oriented deeper into the active site cavity, intercalating between helices B', C, and the N-terminal portion of helix I. We wished to compare the structure of **4c** to ascertain which conformation this scaffold would adopt. We therefore performed cocrystallization of *T. cruzi* CYP51 in complex with compound **4c**, and observed that **4c** binds to the heme, as VNF and posaconazole do, and the vector of **4c** follows that of VNF (Figure 6). Table 5 summarizes the diffraction and refinement statistics; electron density maps for the inhibitor area are presented in the Supporting Information (Figure S3).

DISCUSSION AND CONCLUSIONS

Scaffold Refinement. We began our exploration of the series of imidazole-containing HTS hits by simply installing a ring that restricted compound flexibility. This first round of modification led immediately to **4c**, a potent inhibitor of *T. cruzi* growth that has 169-fold selectivity over host cells. Exploration of the structural substitution of the diaryl ether and replacements of the imidazole heterocycle confirmed that **4c** was already of optimal properties for this scaffold for potency. Although analog **4a** was of equal potency to **4c**, we deprioritized this structure due to the aryl nitro group, which is often cited as a toxicophoric motif that generates reactive oxygen species in vivo.¹⁶ Compound **4j** also showed modestly improved activity, selectivity, and ligand efficiency over **4c**, although we had concerns about the metabolic stability of the benzyl ether motif. We therefore focused on **4c** as a tool to characterize the mechanism of action of this class of growth inhibitors and to better understand the binding modality.

Further study of the in vitro ADME properties of **4c** uncovered further shortcomings of this scaffold that will be directive of future optimization efforts. Importantly, although we are confident in the imidazole functionality's importance to *T. cruzi* CYP51 binding, much work remains for optimization of the central phenyl scaffold combined with other replacements of the 4-chloro-3,5-dimethylphenyl tail group. We anticipate that these further modifications can be aptly informed by the rich structural biology information we have uncovered.

Inhibitor Affinity of *T. cruzi* CYP51. All four tested compounds produce the characteristic type 2 spectral responses in *T. cruzi* CYP51,¹⁷ the Soret band maximum of the hemoprotein shifting from 417 to 424 nm, which is indicative of the formation of the coordination bond between the heme iron and the N3 atom of an imidazole ring. The apparent *K_d* values shown in Table 4 suggested **4c** as the strongest ligand among those tested, the saturation being achieved at an approximately equimolar ratio to enzyme. The apparent binding affinity of **4c** correlates well with its inhibitory effect on the *T. cruzi* CYP51 activity. We observed only a 7.5% substrate conversion at a 2-fold molar excess of the inhibitor over the enzyme (1 h of reaction), indicating a very high

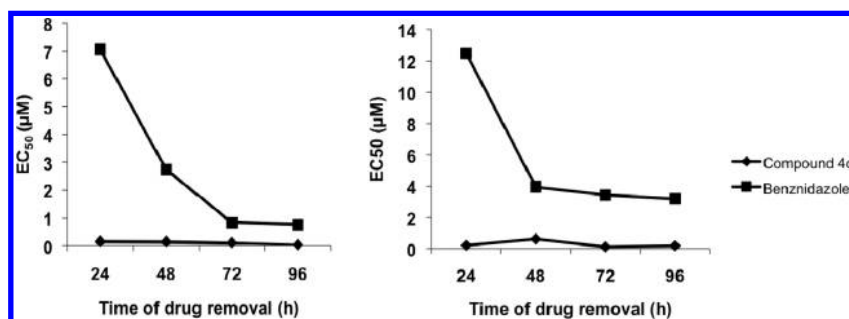


Figure 2. Reversibility of compound **4c**. *T. cruzi* growth inhibition assays were performed by adding the compounds **4c** or benznidazole at the time of infection and washing them off at the indicated times. EC₅₀ was calculated for each condition after 96 h of incubation. Left panel shows *T. cruzi* Tulahuen, and right panel shows *T. cruzi* Y strains.

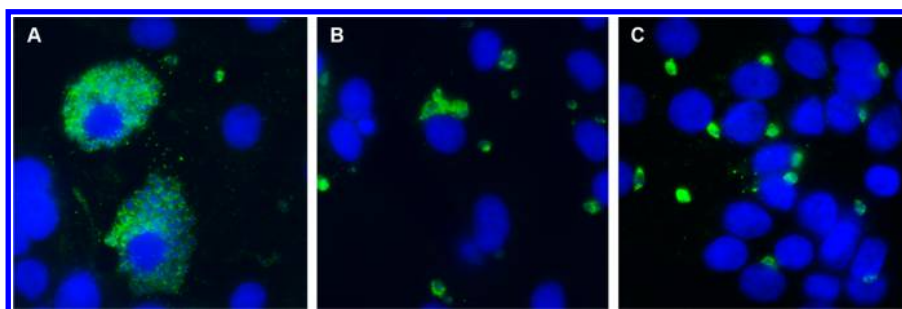


Figure 3. NIH-3T3 fibroblasts were incubated with *T. cruzi* trypomastigotes for 2 h before washing of extracellular *T. cruzi* and addition of drugs. Cells were incubated for 3 days, and stained with an anti-*T. cruzi* antibody and DAPI to visualize DNA. Control infection (A) or infection in the presence of benznidazole (B) and **4c** (C) at 9.5 and 0.4 μM, respectively (5 times the EC₅₀ concentration). These are representative images from a total of 50 fields observed in each condition.

Table 3. In Vitro ADME Parameters for 4c

microsomal stability (%) ^a	
mouse	29
rat	36
human	39
plasma protein binding (%)	
mouse	>99.8
human	>99.8
plasma stability (%) ^b	
mouse	4
human	−9.7
hERG affinity (%)	
	19 (1 μM)
	94 (10 μM)
Caco-2 permeability (nm s ^{−1})	
	209.7

^aPercent metabolized at 20 min. ^bMean percent of difference between C₀ and C_{4h}.

potency that is approaching the potencies of VNF and posaconazole (Table 4 and Figure S4 in the Supporting Information).¹⁸

X-ray Cocystal Structure of 4c Complexed with *T. cruzi* CYP51. The goal of this structural work was to uncover the molecular basis for the observed high inhibitory potency of **4c** as well as to gain further information on possible directions for the future scaffold enhancement. Figure 6a and b depicts an overall view of the enzyme–inhibitor complex and an enlarged view of the inhibitor binding area, respectively. As anticipated, in the *T. cruzi* CYP51 active site, the imidazole ring on **4c** coordinates to the heme iron, the distance between Fe and N3 being only 2.05 Å, while the nonligated 4-chloro-3,5-dimethylphenyl region of the molecule occupies the deepest hydrophobic pocket¹⁹ formed by the distal surface of the heme

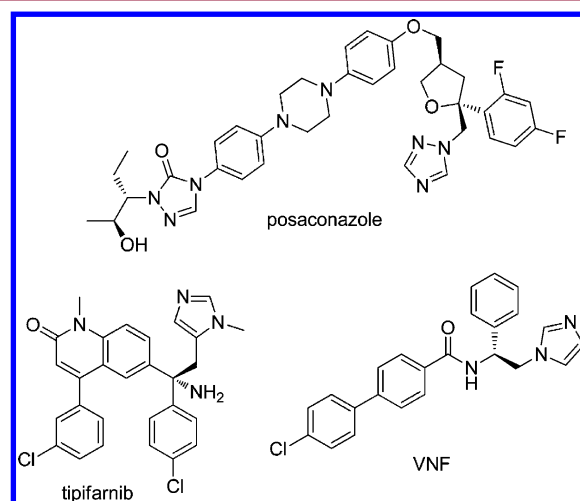


Figure 4. Other azole-based inhibitors of *T. cruzi* CYP51.

plane, the B'C loop (residues F110, A115, and Y116 in Figure 6b), the C-helix (Q120, M123, L127, and L130), and the N-terminal portion of helix I (M284, A287, A288, A291, and T295). Thus, of the 13 amino acid residues forming van der Waals contacts with **4c**, 12 are provided by these three secondary structural elements. Only one inhibitor-contacting residue, L356, derives from the substrate access channel area (K/β1–4 loop, CYP51 SRS5).²⁰

Interestingly, the location of **4c** in the cocystal structure is highly similar to that of VNF (Figure 6c), the CYP51 inhibitor that so far has been the only example of a ligand molecule whose orientation inside the CYP51 binding site cavity is opposite to that of posaconazole (Figure 6d),¹⁸ the VNF analog

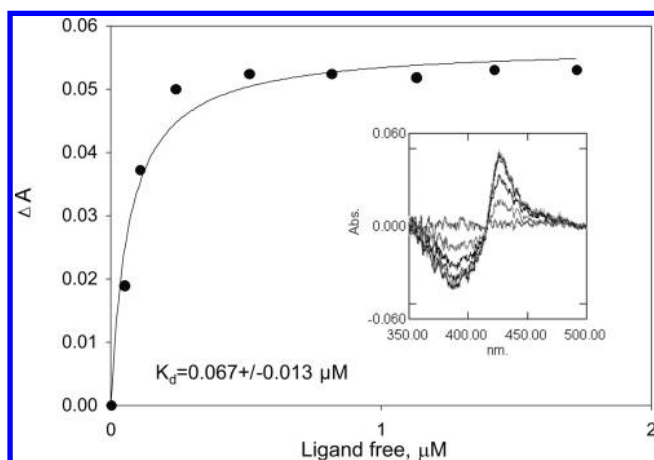


Figure 5. Spectroscopic assay data for **4c** binding to *T. cruzi* CYP51.

Table 4. Binding of Compounds to Recombinant *T. cruzi* CYP51

number	K_d	LE
4c	0.067	0.33
4h	0.18	0.34
4b	0.21	0.32
VNF	0.07	0.25
posaconazole	0.06	0.14

VNI,²¹ or the tipifarnib derivative JK35.²² Moreover, binding of both VNF and **4c** requires shifting of the side chain of Y116 away from the heme, thus causing loss of the hydrogen bond between the Y116 hydroxyl and the porphyrin ring B propionate.²³ This is an interaction conserved in the CYP51 family that is known to play a role in maintaining a catalytically favorable heme environment. Disruption of this heme support from the protein moiety may be one of the reasons for the elevated inhibitory potencies of these relatively small molecules.

In summary, hit-to-lead chemistry follow-up efforts were launched following a phenotypic high-throughput screen, leading to identification of a new, ligand-efficient series of *T. cruzi* growth inhibitors that mediate their effect via inhibition of *T. cruzi* CYP51. Early structure–activity relationships have been outlined, as well as structural biology information that will drive further optimization efforts, which will be reported in due course.

EXPERIMENTAL SECTION

Chemical Synthesis. Unless otherwise noted, reagents were obtained from Sigma-Aldrich, Inc. (St. Louis, MO), or Frontier Scientific Services, Inc. (Newark, DE), and were used as received. Boronic acids and aniline reagents were purchased, unless the synthesis is specifically described below. Reaction solvents were purified by passage through alumina columns on a purification system manufactured by Innovative Technology (Newburyport, MA). Microwave reactions were performed using a Biotage Initiator-8 instrument. NMR spectra were obtained with Varian NMR systems, operating at 400 or 500 MHz for ¹H acquisitions as noted. LCMS analysis was performed using a Waters Alliance reverse-phase HPLC, with single-wavelength UV–visible detector and LCT Premier time-of-flight mass spectrometer (electrospray ionization). All newly synthesized compounds that were submitted for biological testing were deemed >95% pure by LCMS analysis (UV and ESI–MS detection) prior to submission for biological testing. Preparative LCMS was performed on a Waters FractionLynx system with a Waters MicroMass ZQ mass spectrometer (electrospray ionization) and a single-wavelength UV–

visible detector, using acetonitrile/H₂O gradients with 0.1% formic acid. Fractions were collected on the basis of triggering using UV and mass detection. Yields reported for products obtained by preparative HPLC represent the amount of pure material isolated; impure fractions were not repurified.

N-(3-((1*H*-imidazol-1-yl)methyl)phenyl)-2-methyl-4-nitroaniline (4a**).** Compound **7** (0.020 g, 0.084 mmol) dissolved in DMF (0.5 mL) was added to 2-methyl-4-nitroaniline (19.25 mg, 0.127 mmol), Pd₂(dba)₃ (15.45 mg, 0.017 mmol), 2,2′-oxybis(2,1-phenylene)bis(diphenylphosphine) (18.17 mg, 0.034 mmol), and potassium *tert*-butoxide (0.169 mL, 0.169 mmol). The reaction was run for 20 min in the microwave at 170 °C. The crude mixture was diluted with H₂O, and the aqueous layer was extracted with EtOAc (3×). The combined organic layers were washed with brine, dried under anhydrous sodium sulfate, and concentrated. The crude product was purified via preparative HPLC to give **4a** (yield: 40%). ¹H NMR (500 MHz, CDCl₃): δ 8.08 (d, *J* = 2.44 Hz, 1H), 7.98 (dd, *J* = 2.44, 8.79 Hz, 1H), 7.59 (s, 1H), 7.37 (t, *J* = 7.75 Hz, 1H), 7.17 (d, *J* = 7.81 Hz, 1H), 7.13 (s, 1H), 7.07 (d, *J* = 9.28 Hz, 1H), 6.93–6.98 (m, 2H), 6.89 (s, 1H), 5.88 (br s, 1H), 5.14 (s, 2H), 2.33 (s, 3H). LCMS found 309.01, [*M* + *H*]⁺.

3-((1*H*-imidazol-1-yl)methyl)-*N*-(3-methoxyphenyl)aniline (4b**).** Compound **7** (0.0437 g, 0.184 mmol) dissolved in DMF (1 mL) was added to 3-methoxyaniline (0.031 mL, 0.276 mmol), Pd₂(dba)₃ (33.8 mg, 0.037 mmol), 2,2′-oxybis(2,1-phenylene)bis(diphenylphosphine) (39.7 mg, 0.074 mmol), and potassium *tert*-butoxide (0.369 mL, 0.369 mmol). The reaction was heated for 20 min in the microwave at 170 °C. The crude mixture was diluted with H₂O, and the aqueous layer was extracted with EtOAc (3×). The combined organic layers were washed with brine, dried under anhydrous sodium sulfate, and concentrated. The crude product was purified via preparative HPLC to give **4b** (yield: 54%). ¹H NMR (400 MHz, CDCl₃): δ 7.60 (s, 1H), 7.24 (t, *J* = 8.06 Hz, 1H), 7.18 (t, *J* = 8.06 Hz, 1H), 7.11 (s, 1H), 7.02–7.07 (m, 1H), 6.94 (s, 1H), 6.82 (s, 1H), 6.71 (d, *J* = 7.33 Hz, 1H), 6.60–6.66 (m, 2H), 6.52 (dd, *J* = 1.83, 8.43 Hz, 1H), 5.81 (br s, 1H), 5.07 (s, 2H), 3.78 (s, 3H). LCMS found 280.01, [*M* + *H*]⁺.

1-(3-(4-chloro-3,5-dimethylphenoxy)benzyl)-1*H*-imidazole (4c**).** Compound **7** (0.6403 g, 2.70 mmol) dissolved in DMF (8 mL) was added to copper(I) iodide (257 mg, 1.350 mmol), 4-chloro-3,5-dimethylphenol (634 mg, 4.05 mmol), cesium carbonate (1760 mg, 5.40 mmol), and 2-(dimethylamino)acetic acid (418 mg, 4.05 mmol). The reaction was heated for 20 min in the microwave at 180 °C. The crude mixture was diluted with H₂O, and the aqueous layer was extracted with EtOAc (6×). The combined organic layers were washed with brine, dried under anhydrous sodium sulfate, and concentrated. The crude product was purified via preparative HPLC to give **4c** (yield: 40%). ¹H NMR (500 MHz, CDCl₃): δ 7.54 (s, 1H), 7.29 (t, *J* = 7.81 Hz, 1H), 7.10 (s, 1H), 6.89–6.94 (m, 2H), 6.86 (d, *J* = 7.81 Hz, 1H), 6.80 (s, 1H), 6.73 (s, 2H), 5.08 (s, 2H), 2.34 (s, 6H). LCMS found 313.01, [*M* + *H*]⁺.

1-(3-(Biphenyl-3-yloxy)benzyl)-1*H*-imidazole (4d**).** Compound **7** (0.020 g, 0.084 mmol) dissolved in DMF (5 mL) was added to copper(I) iodide (8.03 mg, 0.042 mmol), 3-phenylphenol (21.54 mg, 0.127 mmol), cesium carbonate (55.0 mg, 0.169 mmol), and 2-(dimethylamino)acetic acid (13.05 mg, 0.127 mmol). The reaction was heated for 20 min in the microwave at 180 °C. The crude mixture was diluted with H₂O, and the aqueous layer was extracted with EtOAc (3×). The combined organic layers were washed with brine, dried under anhydrous sodium sulfate, and concentrated. The crude product was purified via preparative HPLC to give **4d** (yield: 5%). ¹H NMR (500 MHz, CDCl₃): δ 8.58 (br s, 1H), 7.52–7.63 (m, 2H), 7.32–7.49 (m, 7H), 7.24–7.26 (m, 1H), 7.04–7.13 (m, 2H), 7.00 (d, *J* = 6.84 Hz, 1H), 6.93 (br s, 2H), 5.22 (br s, 2H). LCMS found 327.01, [*M* + *H*]⁺.

1-(3-(3,5-Dimethylphenoxy)benzyl)-1*H*-imidazole (4e**).** Compound **7** (30 mg, 0.127 mmol) dissolved in DMF (0.8 mL) was added to copper(I) iodide (12.05 mg, 0.063 mmol), 3,5-dimethylphenol (23.19 mg, 0.190 mmol), cesium carbonate (82 mg, 0.253 mmol), and 2-(dimethylamino)acetic acid (19.57 mg, 0.190 mmol). The reaction

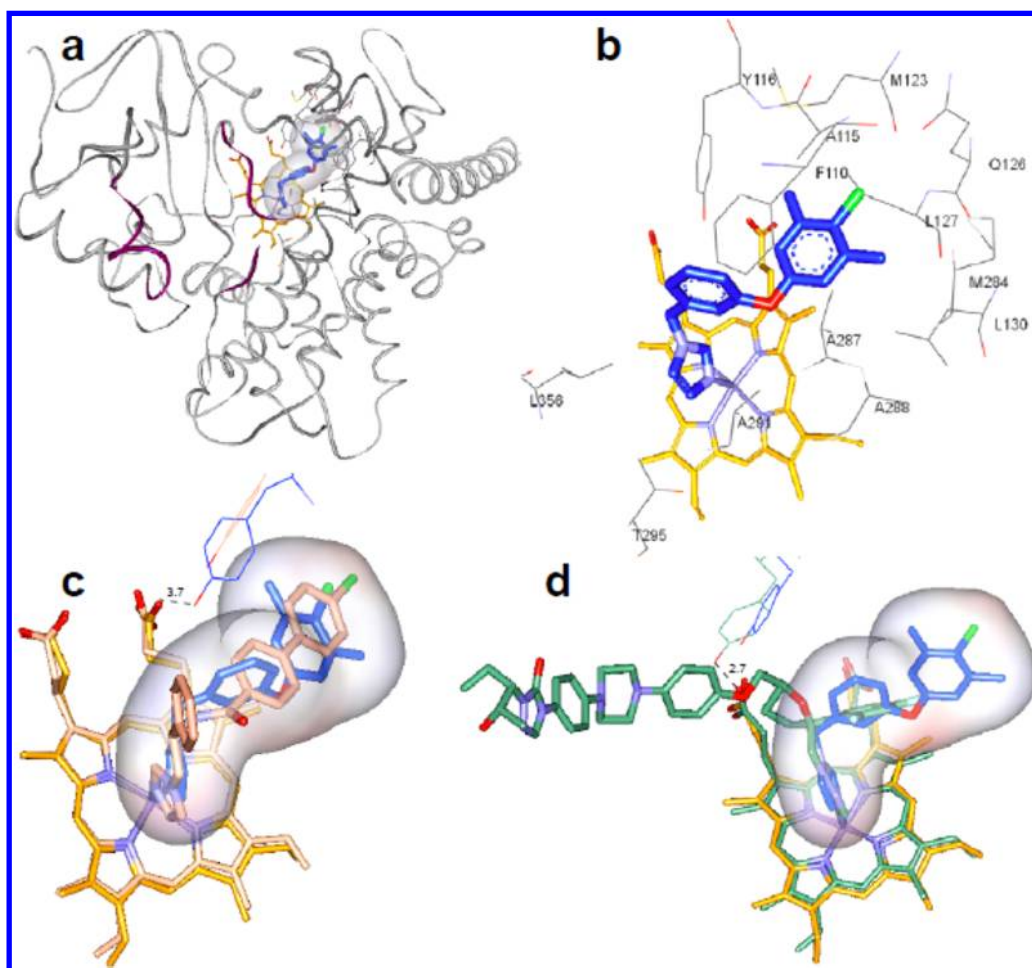


Figure 6. X-ray structure of *T. cruzi* CYP51 complexed to **4c** (PDB code 4H6O). Electron density maps and stereoview of the active site are available in the Supporting Information. (a) Overall view from the distal side of the CYP51 molecule. The polypeptide chain is depicted as a ribbon diagram, and the secondary structural elements forming the substrate access channel entrance are colored in purple. The C atoms of the heme and **4c** are displayed as orange and blue stick models, respectively. The semitransparent surface of **4c** (probe radius 1.4 Å) is colored by interpolated charge. (b) Enlarged view of **4c** in the *T. cruzi* CYP51 active site. The 13 residues located within 4.5 Å from the inhibitor are depicted by lines and labeled. (c) Superimposed cocrystal structures of *T. cruzi* CYP51 with **4c** and VNF (PDB code 3KSW). VNF and the heme from the 3KSW structure are colored in salmon. The distance between the heme ring propionate and OH of Y116 (3.7 Å, dashed line) is 1 Å longer than in the ligand-free or posaconazole-bound CYP51 structures (2.7 Å). (d) Superimposed cocrystal structures of *T. cruzi* CYP51 with **4c** and posaconazole (PDB code 3K1O). Posaconazole, heme, and Y116 from the 3K1O structure are colored in green. VNF and compound **4c** both adopt the orientation in the CYP51 active site, which is opposite to the orientation of posaconazole.

was heated for 20 min in the microwave at 180 °C. The crude mixture was diluted with H₂O, and the aqueous layer was extracted with EtOAc (6×). The combined organic layers were washed with brine, dried under anhydrous sodium sulfate, and concentrated. The crude product was purified via preparative HPLC, followed by further purification via silica gel chromatography (100% hexanes, followed by 10% MeOH in DCM) to give **4e** (yield: 2%). ¹H NMR (500 MHz, CDCl₃): δ 7.54 (br s, 1H), 7.28 (t, *J* = 8.00 Hz, 1H), 7.09 (br s, 1H), 6.90–6.92 (m, 2H), 6.83 (d, *J* = 8.00 Hz, 1H), 6.81 (s, 1H), 6.76 (s, 1H), 6.61 (s, 2H), 5.09 (s, 2H), 2.29 (s, 6H). LCMS found 279.01, [M + H]⁺.

1-(3-(*m*-Tolyloxy)benzyl)-1*H*-imidazole (4f). Compound **7** (65.8 mg, 0.277 mmol) dissolved in DMF (1.2 mL) was added to copper(I) iodide (26.4 mg, 0.139 mmol), *m*-cresol (0.044 mL, 0.416 mmol), cesium carbonate (181 mg, 0.555 mmol), and 2-(dimethylamino)acetic acid (42.9 mg, 0.416 mmol). The reaction was heated for 20 min in the microwave at 180 °C. The crude mixture was diluted with H₂O, and the aqueous layer was extracted with DCM (5×). The combined organic layers were washed with brine, dried under anhydrous sodium sulfate, and concentrated. The crude product was purified via preparative HPLC to give **4f** (yield: 1%). ¹H NMR (400 MHz, CDCl₃): δ 7.64 (br s, 1H), 7.29 (t, *J* = 7.69 Hz, 1H), 7.22

(t, *J* = 7.69 Hz, 1H), 7.12 (br s, 1H), 6.89–6.97 (m, 3H), 6.76–6.88 (m, 4H), 5.09 (s, 2H), 2.33 (s, 3H). LCMS found 265.16, [M + H]⁺.

1-(3-(4-Chlorophenoxy)benzyl)-1*H*-imidazole (4g). Compound **7** (30 mg, 0.127 mmol) dissolved in DMF (0.8 mL) was added to copper(I) iodide (12.05 mg, 0.063 mmol), 4-chlorophenol (24.40 mg, 0.190 mmol), cesium carbonate (82 mg, 0.253 mmol), and 2-(dimethylamino)acetic acid (19.57 mg, 0.190 mmol). The reaction was heated for 20 min in the microwave at 180 °C. The crude mixture was diluted with H₂O, and the aqueous layer was extracted with EtOAc (6×). The combined organic layers were washed with brine, dried under anhydrous sodium sulfate, and concentrated. The crude product was purified via preparative HPLC, followed by further purification via silica gel chromatography (100% hexanes, followed by 10% MeOH in DCM) to give **4g** (yield: 6%). ¹H NMR (500 MHz, CDCl₃): δ 7.54 (s, 1H), 7.28–7.34 (m, 3H), 7.10 (s, 1H), 6.90–6.95 (m, 4H), 6.88 (d, *J* = 7.32 Hz, 1H), 6.81 (s, 1H), 5.09 (s, 2H). LCMS found 285.01, [M + H]⁺.

1-(3-(*o*-Tolyloxy)benzyl)-1*H*-imidazole (4h). Compound **7** (0.040 g, 0.169 mmol) dissolved in DMF (1 mL) was added to copper(I) iodide (16.07 mg, 0.084 mmol), *o*-cresol (27.4 mg, 0.253 mmol), cesium carbonate (110 mg, 0.337 mmol), and 2-(dimethylamino)acetic acid (26.1 mg, 0.253 mmol). The reaction

Table 5. Data Collection and Refinement Statistics for *T. cruzi* CYP51, in Complex with 4a (PDB Code 4H6O)

Data Collection	
wavelength, Å	0.9786
space group	P3(1)21
cell dimensions	
<i>a</i> , <i>b</i> , <i>c</i> , Å	63.290, 63.290, 223.995
α , β , γ , deg	90.00, 90.00, 120.00
molecules per asymmetric unit	
solvent content, %	52.5
resolution (last shell), Å	30–2.55 (2.64–2.55)
<i>R</i> _{merge} (last shell)	0.047 (0.610)
<i>I</i> / σ (last shell)	39.3 (2.9)
completeness (last shell), %	99 (100)
redundancy (last shell)	8.8 (6.0)
Refinement	
resolution, Å	27.5–2.8
<i>R</i> -factor	0.263
<i>R</i> -free	0.275
reflections used	12 800
test set size, %	5.3
rms deviations from ideal geometry	
bond lengths, Å	0.007
bond angles, deg	1.87
Ramachandran plot	
residues in favorable regions (%)	97.2
residues in allowed regions (%)	100
outliers (%)	0
Model	
total number of atoms (average <i>B</i> -factor, Å)	3592 (75.3)
residues	
protein	435 (75.1)
heme	1 (34.9)
4c (NEE)	1 (45.5)
water	55 (86.9)

was heated for 20 min in the microwave at 180 °C. The crude mixture was diluted with H₂O, and the aqueous layer was extracted with EtOAc (6×). The combined organic layers were washed with brine, dried under anhydrous sodium sulfate, and concentrated. The crude product was purified via silica gel chromatography to give **4h** (yield: 33%). ¹H NMR (400 MHz, CDCl₃): δ 7.56 (br s, 1H), 7.24–7.28 (m, 2H), 7.15–7.20 (m, 1H), 7.05–7.12 (m, 2H), 6.86–6.94 (m, 2H), 6.80 (d, *J* = 7.50 Hz, 2H), 6.74 (s, 1H), 5.07 (s, 2H), 2.20 (s, 3H). LCMS found 265.01, [M + H]⁺.

1-(3-Phenoxybenzyl)-1*H*-imidazole (4i). Compound **7** (30 mg, 0.127 mmol) dissolved in DMF (0.8 mL) was added to copper(I) iodide (12.05 mg, 0.063 mmol), phenol (17.86 mg, 0.190 mmol), cesium carbonate (82 mg, 0.253 mmol), and 2-(dimethylamino)acetic acid (19.57 mg, 0.190 mmol). The reaction was heated for 20 min in the microwave at 180 °C. The crude mixture was diluted with H₂O, and the aqueous layer was extracted with EtOAc (6×). The combined organic layers were washed with brine, dried under anhydrous sodium sulfate, and concentrated. The crude product was purified via preparative HPLC, followed by further purification via silica gel chromatography (100% hexanes, followed by 10% MeOH in DCM) to give **4i** (yield: 5%). ¹H NMR (500 MHz, CDCl₃): δ 7.54 (s, 1H), 7.35 (t, *J* = 8.06 Hz, 2H), 7.30 (t, *J* = 8.06 Hz, 1H), 7.13 (t, *J* = 7.57 Hz, 1H), 7.09 (s, 1H), 6.99 (d, *J* = 7.81 Hz, 2H), 6.93 (dd, *J* = 1.95, 8.30 Hz, 1H), 6.91 (s, 1H), 6.86 (d, *J* = 7.81 Hz, 1H), 6.83 (s, 1H), 5.08 (s, 2H). LCMS found 251.01, [M + H]⁺.

1-(3-((4-Chlorobenzyl)oxy)benzyl)-1*H*-imidazole (4j). To **11a** (106 mg, 0.34 mmol) dissolved in DMF (3 mL) were added potassium carbonate (195 mg, 1.41 mmol) and imidazole (97 mg, 1.43 mmol). The mixture was stirred and heated to 100 °C for 1 h. The

mixture was cooled to room temperature, diluted with H₂O (25 mL), and the aqueous layer was extracted with EtOAc (5 × 20 mL). The combined organic layers were washed with H₂O (3 × 15 mL), washed with brine (15 mL), dried under anhydrous sodium sulfate, and concentrated. The crude product was then purified by flash column chromatography using a gradient of 0–1% MeOH in EtOAc to give **4j** as a white solid (yield: 68%). ¹H NMR (500 MHz, CDCl₃): δ ppm 7.55 (s, 1H), 7.31–7.38 (m, 4H), 7.28 (t, *J* = 7.8 Hz, 1H), 7.10 (s, 1H), 6.88–6.92 (m, 2H), 6.77 (d, *J* = 7.8 Hz, 1H), 6.70 (t, *J* = 2.0 Hz, 1H), 5.09 (s, 2H), 4.99 (s, 2H). LCMS found 299.24, [M + H]⁺.

1-(3-(4-Chlorophenethoxy)benzyl)-1*H*-imidazole (4k). To **11b** (107 mg, 0.33 mmol) dissolved in DMF (3 mL) were added potassium carbonate (188 mg, 1.36 mmol) and imidazole (92 mg, 1.35 mmol). The mixture was stirred and heated to 100 °C for 1 h. The mixture was cooled to room temperature, diluted with H₂O (25 mL), and the aqueous layer was extracted with EtOAc (5 × 20 mL). The combined organic layers were washed with H₂O (3 × 15 mL), washed with brine (15 mL), dried under anhydrous sodium sulfate, and concentrated. The crude product was then purified by flash column chromatography using a gradient of 0–1% MeOH in EtOAc to give **4k** as a clear oil (yield: 53%). ¹H NMR (500 MHz, CDCl₃): δ ppm 7.54 (s, 1H), 7.29 (d, *J* = 8.3 Hz, 2H), 7.25 (d, *J* = 7.8 Hz, 1H), 7.20 (dt, *J* = 8.3, 2.4 Hz, 2H), 7.10 (s, 1H), 6.90 (s, 1H), 6.83 (dd, *J* = 8.3, 2.4 Hz, 1H), 6.74 (d, *J* = 7.8 Hz, 1H), 6.64 (t, *J* = 2.0 Hz, 1H), 5.07 (s, 2H), 4.11 (t, *J* = 6.6 Hz, 2H), 3.04 (t, *J* = 6.8 Hz, 2H). LCMS found 313.25, [M + H]⁺.

1-(3-Bromobenzyl)-1*H*-imidazole (7). To **6** (1.50 g, 6.00 mmol) were added imidazole (899 mg, 13.20 mmol) and DMF (15 mL). The reaction was heated for 10 min in the microwave at 180 °C. The crude mixture was then diluted with H₂O, and the aqueous layer was extracted with DCM (5×). The combined organic layers were washed with brine, dried under anhydrous sodium sulfate, and concentrated. The crude product was purified via silica gel chromatography, eluting with 0–5% MeOH in DCM to give **7** as a yellow oil (yield: 55%). ¹H NMR (500 MHz, CDCl₃): δ 7.55 (s, 1H), 7.46 (d, *J* = 7.81 Hz, 1H), 7.30 (s, 1H), 7.23 (t, *J* = 8.06 Hz, 1H), 7.12 (s, 1H), 7.07 (d, *J* = 7.32 Hz, 1H), 6.90 (s, 1H), 5.10 (s, 2H). LCMS found 237.01, [M + H]⁺.

Methyl 3-((4-Chlorobenzyl)oxy)benzoate (9a). To methyl 3-hydroxybenzoate (620 mg, 4.07 mmol) dissolved in DMF (4 mL) were added 4-chlorobenzyl bromide (763 mg, 3.71 mmol) and potassium carbonate (560 mg, 4.05 mmol). The mixture was stirred and heated to 60 °C for 1 h. The crude mixture was diluted with H₂O (25 mL), and the aqueous layer was extracted with a 1:1 mixture of EtOAc and hexanes (3 × 25 mL). The combined organic layers were washed with H₂O (30 mL), washed with brine (20 mL), dried under anhydrous sodium sulfate, and concentrated. The crude product was then purified by flash column chromatography using a gradient of 1–20% EtOAc in hexanes to give **9a** as a white solid (yield: 84%). ¹H NMR (500 MHz, CDCl₃): δ ppm 7.67 (dt, *J* = 7.8, 1.2 Hz, 1H), 7.64 (dd, *J* = 2.4, 1.5 Hz, 1H), 7.34–7.41 (m, 5H), 7.16 (ddd, *J* = 8.3, 2.9, 1.0 Hz, 1H), 5.08 (s, 2H), 3.92 (s, 3H). LCMS found 277.25, [M + H]⁺.

Methyl 3-(4-Chlorophenethoxy)benzoate (9b). To methyl 3-hydroxybenzoate (630 mg, 4.14 mmol) dissolved in DMF (4 mL) were added 1-(2-bromoethyl)-4-chlorobenzene (3.87 g, 17.63 mmol) and potassium carbonate (2.90 g, 20.98 mmol). The mixture was stirred and heated to 60 °C for 4 h. The crude mixture was diluted with H₂O (40 mL), and the aqueous layer was extracted with a 1:1 mixture of EtOAc and hexanes (3 × 40 mL). The combined organic layers were washed with H₂O (30 mL), washed with brine (20 mL), dried under anhydrous sodium sulfate, and concentrated. The crude product was then purified by flash column chromatography using a gradient of 1–20% EtOAc in hexanes to give **9b** as a white solid (yield: 59%). ¹H NMR (500 MHz, CDCl₃): δ ppm 7.64 (d, *J* = 7.8 Hz, 1H), 7.55 (dd, *J* = 2.4, 1.5 Hz, 1H), 7.34 (t, *J* = 8.1 Hz, 1H), 7.30 (dt, *J* = 8.3, 2.0 Hz, 2H), 7.23 (dt, *J* = 8.3, 2.0 Hz, 2H), 7.09 (ddd, *J* = 8.3, 2.9, 1.0 Hz, 1H), 4.20 (t, *J* = 6.6 Hz, 2H), 3.92 (s, 3H), 3.08 (t, *J* = 6.8 Hz, 2H). LCMS found 291.28, [M + H]⁺.

(3-((4-Chlorobenzyl)oxy)phenyl)methanol (10a). **9a** (794 mg, 2.87 mmol) was dissolved in anhydrous THF (6 mL) and cooled to 0

°C. Lithium aluminum hydride (218 mg, 5.74 mmol) was then added slowly, and the mixture was stirred for 15 min. The mixture was warmed to room temperature and was stirred for 45 min. The mixture was cooled to 0 °C and was quenched by the dropwise addition with H₂O (0.3 mL), 15% aqueous KOH (0.3 mL), and H₂O (0.6 mL). The mixture was warmed to room temperature and stirred for 15 min. Magnesium sulfate was added, and the mixture was stirred a further 15 min. The solids were vacuum filtered, and to the filtrate were added H₂O (20 mL), EtOAc (10 mL), and hexanes (10 mL). The organic layer was removed, and the aqueous layer was extracted with EtOAc (3 × 15 mL). The combined organic layers were washed with brine (10 mL), dried under anhydrous sodium sulfate, and concentrated onto silica. The crude product was then purified by flash column chromatography using a gradient of 10–30% EtOAc in hexanes to give **10a** as a white solid (yield: 71%). ¹H NMR (500 MHz, CDCl₃): δ ppm 7.26–7.40 (m, 5H), 7.01 (s, 1H), 6.97 (d, *J* = 7.3 Hz, 1H), 6.89 (dd, *J* = 8.1, 2.7 Hz, 1H), 5.05 (s, 2H), 4.67 (s, 2H), 1.81 (br s, 1H). LCMS found 231.22, [M + H – H₂O]⁺.

(3-(4-Chlorophenethoxy)phenyl)methanol (10b). Compound **9b** (681 mg, 2.34 mmol) was dissolved in anhydrous THF (5 mL) and cooled to 0 °C. Lithium aluminum hydride (190 mg, 5.01 mmol) was then added slowly, and the mixture was stirred for 15 min. The mixture was then warmed to room temperature and was stirred for 45 min. The mixture was cooled to 0 °C and was quenched by the dropwise addition with H₂O (0.3 mL), 15% aqueous KOH (0.3 mL), and H₂O (0.6 mL). The mixture was warmed to room temperature and stirred for 15 min. Magnesium sulfate was added, and the mixture was stirred a further 15 min. The solids were vacuum filtered, and to the filtrate were added H₂O (20 mL), EtOAc (10 mL), and hexanes (10 mL). The organic layer was removed, and aqueous layer was extracted with EtOAc (3 × 20 mL). The combined organic layers were washed with brine (15 mL), dried under anhydrous sodium sulfate, and adsorbed onto silica. The crude product was then purified by flash column chromatography using a gradient of 10–30% EtOAc in hexanes to give **10b** as a clear oil (yield: 96%). ¹H NMR (500 MHz, CDCl₃): δ ppm 7.29 (dt, *J* = 8.3, 2.0 Hz, 2H), 7.26 (d, *J* = 7.8 Hz, 1H), 7.23 (dd, *J* = 8.8, 2.0 Hz, 2H), 6.90–6.96 (m, 2H), 6.82 (dd, *J* = 7.8, 2.4 Hz, 1H), 4.67 (s, 2H), 4.17 (t, *J* = 6.8 Hz, 2H), 3.07 (t, *J* = 6.8 Hz, 2H), 1.70 (br. s., 1H). LCMS found 245.25, [M + H – H₂O]⁺.

1-(Bromomethyl)-3-((4-chlorobenzyl)oxy)benzene (11a). Compound **10a** (396 mg, 1.59 mmol) was dissolved in anhydrous THF (8 mL) under a stream of nitrogen. Triphenylphosphine (463 mg, 1.77 mmol) was added, and the solution was stirred for 5 min before the addition of *N*-bromosuccinimide (312 mg, 1.75 mmol). The mixture was stirred at room temperature for 2 h. The reaction was quenched with H₂O (15 mL), and the aqueous mixture was extracted with a 1:1 mixture of hexanes and EtOAc (3 × 15 mL). The combined organic layers were washed with brine (10 mL), dried under anhydrous sodium sulfate, and concentrated. The crude product was then purified by flash column chromatography using a gradient of 0–5% EtOAc in hexanes to give **11a** as a white solid (yield: 86%). ¹H NMR (500 MHz, CDCl₃): δ ppm 7.38 (s, 4H), 7.27 (t, *J* = 8.1 Hz, 1H), 6.99–7.04 (m, 2H), 6.90 (dd, *J* = 8.3, 2.4 Hz, 1H), 5.04 (s, 2H), 4.47 (s, 2H). GCMS found 309.9, [M⁺]

1-(Bromomethyl)-3-(4-chlorophenethoxy)benzene (11b). Compound **10b** (549 mg, 2.09 mmol) was dissolved in anhydrous THF (5 mL) under a stream of nitrogen. Triphenylphosphine (626 mg, 2.39 mmol) was added, and the solution was stirred for 5 min before the addition of *N*-bromosuccinimide (437 mg, 2.46 mmol). The mixture was stirred at room temperature for 2 h. The reaction was quenched with H₂O (20 mL), and the aqueous mixture was extracted with a 1:1 mixture of hexanes and EtOAc (3 × 15 mL). The combined organic layers were washed with brine (15 mL), dried under anhydrous sodium sulfate, and concentrated. The crude product was then purified by flash column chromatography using a gradient of 0–5% EtOAc in hexanes to give **11b** white solid (yield: 88%). ¹H NMR (500 MHz, CDCl₃): δ ppm 7.31 (dt, *J* = 8.3, 2.0 Hz, 2H), 7.22–7.26 (m, 3H), 6.99 (d, *J* = 7.3 Hz, 1H), 6.93 (t, *J* = 2.0 Hz, 1H), 6.84 (dd, *J* = 8.3, 2.4 Hz, 1H), 4.46 (s, 2H), 4.17 (t, *J* = 6.8 Hz, 2H), 3.08 (t, *J* = 6.8 Hz, 2H). GCMS found 323.9, [M⁺]

3-(4-Chloro-3,5-dimethylphenoxy)benzaldehyde (13). 3-Bromobenzaldehyde (1.0 g, 0.630 mL, 5.40 mmol) was dissolved in 1,4-dioxane (40.0 mL), and then 4-chloro-3,5-dimethylphenol (1.270 g, 8.11 mmol), 2-(dimethylamino)acetic acid (0.836 g, 8.11 mmol), cesium carbonate (5.28 g, 16.21 mmol), copper(I) iodide (0.515 g, 2.70 mmol), and other 20 mL of 1,4-dioxane were added to the solution. The reaction was heated to 180 °C. After 4 h, another 0.5 equiv of all of the reagents except the aldehyde were added, and heating continued. After 12 h, the crude was evaporated to dryness and then dissolved in DCM (100 mL). The solution was filtered two times on filter paper. The organic phase was washed with NaOH 10 N solution (2 × 30 mL), and then aqueous layers were washed with DCM (3 × 30 mL). The combined organic layers were washed with brine, dried over anhydrous sodium sulfate, and concentrated. The crude product was purified via silica gel chromatography (9:1 hexane/EtOAc) to give **13** as a yellow oil (1.320 g, 94% yield). ¹H NMR (500 MHz, CDCl₃): δ 9.96 (s, 1H), 7.60 (d, *J* = 7.80 Hz, 1H), 7.50 (t, *J* = 7.80 Hz, 1H), 7.41–7.43 (m, 1H), 7.25–7.28 (m, 1H), 6.78 (s, 2H), 2.36 (s, 6H). LCMS found 261.03, [M + H]⁺.

5-(3-(Bromomethyl)phenoxy)-2-chloro-1,3-dimethylbenzene (14). To a solution of 3-(4-chloro-3,5-dimethylphenoxy)benzaldehyde (807 mg, 3.10 mmol) in CH₃CN (5 mL) was added lithium bromide (512 mg, 5.90 mmol) followed by the dropwise addition of chlorotrimethylsilane (0.786 mL, 6.19 mmol). After 15 min, the reaction mixture was cooled to 0 °C, 1,1,3,3-tetramethyldisiloxane (1.368 mL, 7.74 mmol) was added dropwise, and the resulting mixture was heated to 80 °C overnight. The mixture was separated into two layers. The lower layer was removed, was diluted with DCM, and was filtered through filter paper. The filtrate was concentrated under reduced pressure, was dissolved in DCM, and was refiltered. The solvent was removed in vacuo to provide **14** as a light yellow oil (0.88 g, 87% yield). ¹H NMR (500 MHz, CDCl₃): δ 7.31 (t, *J* = 7.80 Hz, 1H), 7.12 (d, *J* = 7.80 Hz, 1H), 7.00 (t, *J* = 2.40 Hz, 1H), 6.92 (dd, *J* = 2.40, 7.80 Hz, 1H), 6.75 (s, 2H), 4.54 (s, 2H), 2.35 (s, 6H). LCMS found 325.39, [M + H]⁺.

General Alkylation Procedure for Compounds 15a–k. To a solution of **14** (20 mg, 0.061 mmol) in 0.5 mL of DMF was added the appropriate heterocycle in 1 mL of DMF (0.092 mmol), then K₂CO₃ (16.98 mg, 0.123 mmol), and the mixtures were stirred for 3 h at 50 °C. After 3 h, reactions were cooled and filtered through 17 mm cellulose syringe filters (0.45 μm) and purified via preparative HPLC to give the desired products.

1-(3-(4-Chloro-3,5-dimethylphenoxy)benzyl)-1H-1,2,3-triazole (15a). Yield: 25%. ¹H NMR (500 MHz, CDCl₃): δ 7.72 (s, 1H), 7.50 (s, 1H), 7.31 (t, *J* = 8.0 Hz, 1H), 6.91–6.97 (m, 2H), 6.88 (br s, 1H), 6.72 (s, 2H), 5.53 (s, 2H), 2.34 (s, 6H). LCMS found 314.03, [M + H]⁺.

1-(3-(4-Chloro-3,5-dimethylphenoxy)benzyl)-1H-1,2,4-triazole (15b). Yield: 3.1%. ¹H NMR (500 MHz, CDCl₃): δ 8.07 (br s, 1H), 7.97 (s, 1H), 7.31 (t, *J* = 7.80 Hz, 1H), 6.95 (d, *J* = 7.80 Hz, 1H), 6.93 (dd, *J* = 2.40, 7.80 Hz, 1H), 6.87–6.89 (m, 1H), 6.73 (s, 2H), 5.31 (s, 2H), 2.34 (s, 6H). LCMS found 314.00, [M + H]⁺.

1-(3-(4-Chloro-3,5-dimethylphenoxy)benzyl)-1H-pyrazole (15c). Yield: 20%. ¹H NMR (500 MHz, CDCl₃): δ 7.55 (d, *J* = 1.95 Hz, 1H), 7.40 (d, *J* = 1.95 Hz, 1H), 7.29 (t, *J* = 7.80 Hz, 1H), 6.87–6.91 (m, 2H), 6.82 (s, 1H), 6.72 (s, 2H), 6.29 (t, *J* = 1.95 Hz, 1H), 5.30 (s, 2H), 2.33 (s, 6H). LCMS found 312.99, [M + H]⁺.

4-(3-(4-Chloro-3,5-dimethylphenoxy)benzyl)morpholine Formate (15d). Yield: 7%. ¹H NMR (500 MHz, CDCl₃): δ 8.13 (s, 1H), 7.30 (t, *J* = 7.80 Hz, 1H), 7.09 (d, *J* = 7.80 Hz, 1H), 6.99 (br. s, 1H), 6.91 (dd, *J* = 2.40, 7.80 Hz, 1H), 6.74 (s, 2H), 3.79 (t, *J* = 4.64 Hz, 4H), 3.69 (s, 2H), 2.65 (br s, 4H), 2.34 (s, 6H). LCMS found 332.02, [M + H]⁺.

1-(3-(4-Chloro-3,5-dimethylphenoxy)benzyl)-1H-benzo[d]-imidazole (15e). Yield: 17%. ¹H NMR (500 MHz, CDCl₃): δ 8.01 (s, 1H), 7.82–7.85 (m, 1H), 7.26–7.32 (m, 4H), 6.88–6.92 (m, 2H), 6.83 (t, *J* = 2.00 Hz, 1H), 6.69 (s, 2H), 5.33 (s, 2H), 2.32 (s, 6H). LCMS found 362.97, [M + H]⁺.

2-(3-(4-Chloro-3,5-dimethylphenoxy)benzyl)-2H-1,2,3-triazole (15f). Yield: 8%. ¹H NMR (500 MHz, CDCl₃): δ 7.63 (s, 2H),

7.29 (dt, $J = 2.44, 7.80$ Hz, 1H), 6.99 (d, $J = 7.80$ Hz, 1H), 6.88–6.91 (m, 2H), 6.72 (s, 2H), 5.58 (s, 2H), 2.33 (s, 6H). LCMS found 314.00, $[M + H]^+$.

1-(3-(4-Chloro-3-methylphenoxy)benzyl)-4-methylpiperazine (15g). Yield: 7%. ^1H NMR (500 MHz, CDCl_3): δ 7.23–7.28 (m, 1H), 7.06 (d, $J = 7.30$ Hz, 1H), 6.99 (br s, 1H), 6.85 (dt, $J = 2.40, 7.30$ Hz, 1H), 6.73 (s, 2H), 3.49 (s, 2H), 2.46 (br s, 8H), 2.34 (s, 6H), 2.28 (s, 3H). LCMS found 345.04, $[M + H]^+$.

4-(3-(4-Chloro-3,5-dimethylphenoxy)benzyl)-4H-1,2,4-triazole (15h). Yield: 3.1%. ^1H NMR (500 MHz, CDCl_3): δ 8.17 (s, 2H), 7.33 (t, $J = 7.30$ Hz, 1H), 6.95 (dd, $J = 2.40, 7.30$ Hz, 1H), 6.88 (d, $J = 7.30$ Hz, 1H), 6.81–6.83 (m, 1H), 6.73 (s, 2H), 5.14 (s, 2H), 2.35 (s, 6H). LCMS found 314.03, $[M + H]^+$.

1-(3-(4-Chloro-3,5-dimethylphenoxy)benzyl)-1H-indole (15i). Yield: 3.6%. ^1H NMR (500 MHz, CDCl_3): δ 7.64 (d, $J = 7.80$ Hz, 1H), 7.25–7.28 (m, 1H), 7.23 (t, $J = 7.80$ Hz, 1H), 7.17 (t, $J = 7.80$ Hz, 1H), 7.13 (d, $J = 3.40$ Hz, 1H), 7.11 (d, $J = 7.80$ Hz, 1H), 6.80–6.85 (m, 2H), 6.76–6.78 (m, 1H), 6.68 (s, 2H), 6.54 (d, $J = 3.40$ Hz, 1H), 5.29 (s, 2H), 2.31 (s, 6H). LCMS found 362.07, $[M + H]^+$.

2-(3-(4-Chloro-3,5-dimethylphenoxy)benzyl)-2H-indazole (15j). Yield: 6%. ^1H NMR (500 MHz, CDCl_3): δ 7.92 (s, 1H), 7.72 (d, $J = 8.80$ Hz, 1H), 7.64 (d, $J = 8.80$ Hz, 1H), 7.29 (t, $J = 7.80$ Hz, 2H), 7.09 (s, 1H), 6.98 (d, $J = 7.80$ Hz, 1H), 6.89–6.92 (m, 2H), 6.71 (s, 2H), 5.57 (s, 2H), 2.31 (s, 6H). Regiochemistry confirmed by NOE experiments (Supporting Information). LCMS found 362.99, $[M + H]^+$.

1-(3-(4-Chloro-3,5-dimethylphenoxy)benzyl)-1H-indazole (15k). Yield: 3%. ^1H NMR (500 MHz, CDCl_3): δ 8.03 (s, 1H), 7.75 (d, $J = 8.30$ Hz, 1H), 7.33–7.35 (m, 2H), 7.23 (d, $J = 7.81$ Hz, 1H), 7.13–7.17 (m, 1H), 6.90 (d, $J = 7.81$ Hz, 1H), 6.84 (dd, $J = 2.44, 7.80$ Hz, 1H), 6.79–6.81 (m, 1H), 6.67 (s, 2H), 5.57 (s, 2H), 2.30 (s, 6H). LCMS found 362.99, $[M + H]^+$.

General Procedure for Compounds 17. The appropriate ester 16 (2.325 mmol) was dissolved in 1,4-dioxane (20.0 mL), and then 4-chloro-3,5-dimethylphenol (3.49 mmol), 2-(dimethylamino)acetic acid (3.49 mmol), cesium carbonate (4.65 mmol), and copper(I) iodide (1.16 mmol) were added to the solution. The reaction was refluxed in a preheated oil bath at 180 °C. After 9 h, the crude was evaporated to dryness and then dissolved in DCM (70 mL). The solution was filtered on filter paper. The organic phase was washed with Na_2CO_3 5% solution (2×50 mL), and then aqueous layers were washed with DCM (3×30 mL). The combined organic layers were washed with brine, dried under anhydrous Na_2SO_4 , and concentrated. The crude product was purified via silica gel chromatography (9:1 hexane/EtOAc) to give the desired product.

Methyl 3-(4-Chloro-3,5-dimethylphenoxy)benzoate (17a). Yield: 72%. ^1H NMR (500 MHz, CDCl_3): δ 7.78 (d, $J = 7.80$ Hz, 1H), 7.61–7.63 (m, 1H), 7.40 (t, $J = 7.80$ Hz, 1H), 7.18 (dd, $J = 2.45, 8.30$ Hz, 1H), 6.74 (s, 2H), 3.90 (s, 3H), 2.35 (s, 6H). LCMS found 291.0, $[M + H]^+$.

Methyl 2-(3-(4-Chloro-3,5-dimethylphenoxy)phenyl)-acetate. (17b). Yield: 31.5%. ^1H NMR (500 MHz, CDCl_3): δ 7.27–7.29 (m, 1H), 7.01 (d, $J = 7.80$ Hz, 1H), 6.91 (t, $J = 1.95$ Hz, 1H), 6.87 (dd, $J = 1.95, 8.30$ Hz, 1H), 6.75 (s, 2H), 3.70 (s, 2H), 3.59–3.62 (m, 3H), 2.34 (s, 6H). LCMS found 305.10, $[M + H]^+$.

General Procedure for Compounds 18. To a solution of appropriate ester (1.469 mmol) in THF (2 mL) was added lithium hydroxide (2.94 mmol) in H_2O (2 mL). The reaction was stirred at room temperature for 2 h. The reaction was evaporated to dryness and dissolved in H_2O . The mixture was washed with EtOAc (30 mL), and the aqueous was acidified to pH 2–3 with 3 M HCl (10 mL). Product was extracted using EtOAc (4×20 mL), and the solution was dried under anhydrous Na_2SO_4 . The solvent was removed in vacuo to provide the desired product, which was used without further purification.

3-(4-Chloro-3,5-dimethylphenoxy)benzoic Acid (18a). Yield: 87%. ^1H NMR (500 MHz, $\text{DMSO}-d_6$): δ 7.69 (d, $J = 7.8$ Hz, 1H), 7.47 (t, $J = 7.8$ Hz, 1H), 7.42 (m, $J = 1.5$ Hz, 1H), 7.23 (dd, $J = 7.6, 2.2$ Hz, 1H), 6.87 (s, 2H), 2.30 (s, 6H). LCMS found 277.03, $[M + H]^+$.

2-(3-(4-Chloro-3,5-dimethylphenoxy)phenyl)acetic Acid (18b). Yield: 96%. ^1H NMR (500 MHz, CDCl_3): δ 7.29 (t, $J = 7.80$ Hz, 1H), 7.03 (d, $J = 7.80$ Hz, 1H), 6.93 (t, $J = 1.00$ Hz, 1H), 6.89 (dd, $J = 2.40, 8.30$ Hz, 1H), 6.75 (s, 2H), 3.64 (s, 2H), 2.34 (s, 6H). LCMS found 290.58, $[M + H]^+$.

General Procedure for Compounds 19. The appropriate acid 18 (1.19 mmol) was dissolved in DMF (7 mL), and then acetohydrazide (2.39 mmol), HOBT (1.789 mmol), and EDC (1.79 mmol) were added to the solution. The reaction was stirred at room temperature for 5 h. The reaction was evaporated to dryness and solubilized in DCM (20 mL) and H_2O (20 mL). The organic layer was removed, and the aqueous was extracted with DCM (2×20 mL). The combined organic layers were washed with H_2O (20 mL), washed with brine (5 mL), and dried under anhydrous Na_2SO_4 . The solvent was removed in vacuo, and the residue was purified via silica gel chromatography (2% MeOH in DCM) to provide the desired product.

N'-Acetyl-3-(4-chloro-3,5-dimethylphenoxy)benzohydrazide (19a). Yield: 78%. ^1H NMR (500 MHz, CDCl_3): δ 9.78 (br s, 1H), 9.58 (br s, 1H), 7.51 (d, $J = 8.05$ Hz, 1H), 7.43 (t, $J = 2.20$ Hz, 1H), 7.32 (t, $J = 8.05$ Hz, 1H), 7.07–7.11 (m, 1H), 6.71 (s, 2H), 2.32 (s, 6H), 2.02–2.08 (m, 3H). LCMS found 333.03, $[M + H]^+$.

N'-Acetyl-2-(3-(4-chloro-3,5-dimethylphenoxy)phenyl)-acetohydrazide (19b). Yield: 67.1%. ^1H NMR (500 MHz, CDCl_3): δ 8.45–8.55 (br s, 1H), 8.01 (br s, 1H), 7.28 (t, $J = 7.80$ Hz, 1H), 7.02 (d, $J = 7.80$ Hz, 1H), 6.91 (t, $J = 2.00$ Hz, 1H), 6.88 (dd, $J = 2.40, 8.80$ Hz, 1H), 6.74 (s, 2H), 5.30 (s, 2H), 2.94–2.97 (m, 6H), 2.88 (s, 3H). LCMS found 346.5, $[M + H]^+$.

General Procedure for Compounds 20. The appropriate hydrazide (0.120 mmol) was added to POCl_3 (2.164 mmol), and the reaction mixture was heated at reflux (110 °C) for 1 h. The reaction mixture was evaporated to dryness, and the residue was purified via preparative HPLC.

2-(3-(4-Chloro-3,5-dimethylbenzyl)phenyl)-5-methyl-1,3,4-oxadiazole (20a). Yield: 5.3%. ^1H NMR (500 MHz, CDCl_3): δ 7.76 (d, $J = 7.80$ Hz, 1H), 7.60 (t, $J = 1.00$ Hz, 1H), 7.45 (t, $J = 7.80$ Hz, 1H), 7.14 (dd, $J = 2.45, 8.30$ Hz, 1H), 6.78 (s, 2H), 2.61 (s, 3H), 2.36 (s, 6H). LCMS found 313.01, $[M + H]^+$.

2-(3-(4-Chloro-3,5-dimethylphenoxy)benzyl)-5-methyl-1,3,4-oxadiazole (20b). Yield: 2.2%. ^1H NMR (400 MHz, CDCl_3): δ 7.28 (t, $J = 8.05$ Hz, 1H), 7.02 (d, $J = 7.33$ Hz, 1H), 6.92 (t, $J = 2.20$ Hz, 1H), 6.88 (dd, $J = 2.20, 8.05$ Hz, 1H), 6.74 (s, 2H), 4.12 (s, 2H), 2.48 (s, 3H), 2.34 (s, 6H). LCMS found 328.49, $[M + H]^+$.

General Procedure for Compounds 21. To a solution of the appropriate hydrazide (0.096 mmol) in 1,4-dioxane (2 mL) was added Lawesson's Reagent (0.288 mmol) portion-wise, and the reaction mixture was heated at reflux (100 °C) for 2 h. The reaction was evaporated to dryness and solubilized in DCM (20 mL). The solution was washed with a saturated solution of NaHCO_3 (2×20 mL) and brine (1×10 mL). The organic layer was dried under anhydrous Na_2SO_4 . The solvent was removed in vacuo. Reaction mixture was evaporated to dryness, and the residue was purified via preparative HPLC.

2-(3-(4-Chloro-3,5-dimethylphenoxy)phenyl)-5-methyl-1,3,4-thiadiazole (21a). Yield: 2.5%. ^1H NMR (500 MHz, CDCl_3): δ 7.62 (dd, $J = 0.98, 7.81$ Hz, 1H), 7.57 (t, $J = 2.40$ Hz, 1H), 7.41 (t, $J = 8.30$ Hz, 1H), 7.08 (dd, $J = 2.40, 8.30$ Hz, 1H), 6.78 (s, 2H), 2.81 (s, 3H), 2.36 (s, 6H). LCMS found 330.95, $[M + H]^+$.

2-(3-(4-Chloro-3,5-dimethylphenoxy)benzyl)-5-methyl-1,3,4-thiadiazole (21b). Yield: 6.0%. ^1H NMR (500 MHz, CDCl_3): δ 7.28 (t, $J = 8.05$ Hz, 1H), 7.02 (d, $J = 7.32$ Hz, 1H), 6.91 (t, $J = 2.20$ Hz, 1H), 6.88 (dd, $J = 2.20, 8.05$ Hz, 1H), 6.73 (s, 2H), 4.35 (s, 2H), 2.71 (s, 3H), 2.34 (s, 6H). LCMS found 344.49, $[M + H]^+$.

T. cruzi and Mammalian Cells Cultures. LLC-MK2 were used to cultivate *T. cruzi* and NIH/3T3 for infection assay to test compounds activity. Both cell lines were grown in DMEM supplemented with 10% FBS, 100 U/ml penicillin, 0.1 mg/mL streptomycin, and 0.292 mg/mL glutamine (Pen-Strep-Glut) at 37 °C and 5% CO_2 .

T. cruzi Tulahuen strain expressing the β -gal gene (clone C4)²⁴ and *T. cruzi* Y strain expressing the firefly Luciferase gene⁸ were grown on LLC-MK2 cells in DMEM with 2% FBS and 1% Pen-Strep-Glut at 37

°C and 5% CO₂ and harvested every 5–7 days. Trypomastigotes in the harvested medium were centrifuged for 7 min at 2500 rpm. To separate from amastigotes and cellular debris, the trypomastigotes were allowed to swim out of the pellet for at least 3 h at 37 °C.

***T. cruzi* in Vitro Inhibition Assay.** Harvested trypomastigotes were centrifuged and washed with DMEM without phenol red supplemented with 2% FBS and Pen-Strep-Glut. Phenol red interferes with absorbance readings at 590 nm and needs to be avoided. NIH/3T3 host cells (50 000 per well) and purified *T. cruzi* trypomastigotes (50 000 per well) were seeded in 96-well plates. Test compounds were added at a maximum concentration of 50 μM. DMSO was always lower than 0.5%, which does not affect the viability of the parasites. Each determination was performed in duplicated wells. Amphotericin B (Sigma-Aldrich) was used as control to obtain maximal inhibition at a final concentration of 4 μM. Six wells of each negative and positive controls were carried in every plate. The plates were incubated for 96 h before processing. When the assay was performed with *T. cruzi* expressing β-galactosidase,²⁴ 50 μL of PBS with 0.5% NP40 and 100 μM chlorophenol Red-β-D-galactoside (CPRG) (Sigma) were added per well, plates were incubated at 37 °C for 4 h, and absorbance was read at 590 nm. When the assay was performed with *T. cruzi* expressing the firefly Luciferase gene,⁸ D-Luciferin potassium salt dissolved in PBS was added at a final concentration of 150 μg/mL, and luminescence was measured for 1 s right after addition. Both assays were read using a Victor X3 Perkin-Elmer plate reader.

The absorbance or luminescence obtained was proportional to the viability of the parasite. To determine EC₅₀ values, the absorbance or luminescence was converted to the activity anti-*T. cruzi* of the compounds according to the formula: % activity = 100 – 100*[(CPD – CPA)/(CP – CPA)], where CPD = cells + parasites + drug; CPA = cells + parasites + amphotericin B; and CP = cells + parasites. The log of the molar tested concentrations were plotted against the % activity in the Graph Prism Software, and the value of EC₅₀ was determined. EC₅₀ values are relative to the maximal inhibition values, which are obtained when cultures are incubated with amphotericin B (4 μM). These CPA values are significantly lower than the CP controls (typically 7-fold lower), but are higher than the values of cells alone (approximately 2-fold), because there is a background of extracellular trypomastigotes that do not invade host cells and do not die over the 4 days of the assay.

Immunofluorescence Assay. NIH-3T3 cells plated on coverslips were infected with either *T. cruzi* Tulahuen expressing β-galactosidase or *T. cruzi* Y expressing luciferase and incubated with culture medium alone or containing compound **4c** or benznidazole at 5 times the value of the EC₅₀ obtained in the in vitro assay. After 3 days, they were fixed with 4% of paraformaldehyde, rinsed with PBS, permeabilized for 15 min in PBS with 0.1% Triton X-100 (Sigma-Aldrich), and blocked for 20 min in PBS with 10% goat serum, 1% bovine serum albumin, 100 mM glycine, and 0.05% sodium azide. The cells were incubated for 1 h at room temperature with a polyclonal rabbit anti-*T. cruzi* (kindly provided by Dr. Barbara Burleigh, Harvard University, Boston) at 1:2000 dilution. After rinsing, they were incubated for 1 h at a 1:800 dilution with an Alexa Fluor 488 goat antirabbit IgG secondary antibody (Molecular Probes, Invitrogen), followed by DAPI to stain the nuclei. Coverslips were mounted on Mowiol and analyzed using an inverted Olympus IX70 microscope with a 60× oil-immersion objective.

***T. cruzi* in Vitro Reversibility Assay.** This assay was performed with *T. cruzi* Tulahuen expressing β-galactosidase²⁴ and *T. cruzi* Y strain expressing the firefly Luciferase gene.⁸ The same procedures for the *T. cruzi* in vitro inhibition assay were followed, but compound **4c** or benznidazole was washed out from the well and replaced by fresh culture medium at different time points (24, 48, and 72h) after addition of the compounds. After 96 h of incubation, the specific substrates for each strain of parasite were added to the wells, and absorbance or luminescence was read using a Victor X3 Perkin-Elmer plate reader. EC₅₀ values were determined as previously described.

Testing *T. cruzi* CYP51 as a Potential Target for Inhibitor Compounds. Compounds **4b**, **4c**, and **4h** were studied as CYP51 ligand/inhibitors in vitro using purified full-length *T. cruzi* CYP51

protein sample. Binding affinities of the compounds were estimated using spectral titration.¹⁷ The experiments were performed on a dual-beam Shimadzu UV-2401PC spectrophotometer in the wavelength range 350–450 nm at 25 °C in 2 mL tandem cuvettes at 2 μM P450 and ligand concentrations ranging from 0.5 to 10 μM. The apparent dissociation constants were calculated by plotting the absorbance changes in the difference spectra (ΔA_{425–390}) upon titration against free ligand concentration and fitting the data to a rectangular hyperbola in Sigma Plot Statistics. Inhibitory potencies of the compounds were compared in the reconstituted CYP51 reaction,²⁵ 5 min and 1 h, at 50/2/1 molar ratio substrate/inhibitor/enzyme. Posaconazole served as positive control;¹⁸ P450 concentration in the reaction mixture was 1 μM. The reaction products were analyzed on a reverse-phase HPLC system (Waters) equipped with a C18Nova Pak column and a β-RAM detector (INUS Systems, Inc.).²⁰

X-ray Crystallography. Crystallographic studies were carried out using the Δ31 N-terminus truncated expression construct of *T. cruzi* CYP51 (MAKKT-P³²).¹⁸ A 20 mM stock solution of **4c** in DMSO was added to the 300 μM solution of the protein in 20 mM K-phosphate buffer, pH 7.2, containing 200 mM NaCl, 0.1 mM EDTA, 10% glycerol, and 8 mM Cymal 4, to produce the final concentration of 600 μM. Co-crystals were obtained by hanging-drop vapor diffusion at 22 °C against a well solution containing 50 mM K-phosphate buffer, pH 7.6, 0.2 M magnesium chloride hexahydrate, and 25% (w/v) PEG 4000. Data were collected at LS-CAT, Advanced Photon Source, Argonne National Laboratory, beamline 21ID-F, and processed with HKL2000 software package. The structure was determined in CCP4 Program Suite 6.2.0. Solvent content was estimated with Matthews probability calculator. A single solution with one protein monomer in the asymmetric was found with PhaserMR using posaconazole-bound *T. cruzi* CYP51 structure (PDB code 3K1O)¹⁸ as a search model, an initial R_{factor} of 0.44, and log-likelihood gain of 640. Model building and refinement were performed with COOT and REFMAC5, respectively. Table 5 summarizes the diffraction and refinement statistics; electron density maps for the inhibitor area are presented in the Supporting Information (Figure S3). The coordinates and structure factors of *T. cruzi* CYP51 in complex with compound **4c** (PDB ID NEE) have been deposited at the RCSB Protein Data Bank, PDB code 4H6O.

■ ASSOCIATED CONTENT

● Supporting Information

A tabulation of all inhibitors and screening data is publically available as a shared data set at www.collaborativedrugdiscovery.com. Synthetic details and characterization of the compounds described, cross-correlation of the manuscript compound numbers and NEU registration numbers, and the amino acid sequence alignment of *T. cruzi* CYP51 with selected fungal CYP51 orthologs. This material is available free of charge via the Internet at <http://pubs.acs.org>.

Accession Codes

The coordinates and structure factors of *T. cruzi* CYP51 in complex with compound **4c** (PDB ID NEE) have been deposited at the RCSB Protein Data Bank, PDB code 4H6O.

■ AUTHOR INFORMATION

Corresponding Author

*Phone: (617) 373-2703 (M.P.P.); (212) 263-6757 (A.R.); (615) 343-1373 (G.I.L.). E-mail: m.pollastri@neu.edu (M.P.P.); ana.rodriguez@nyumc.org (A.R.); galina.i.lepesheva@vanderbilt.edu (G.I.L.).

Notes

The authors declare no competing financial interest.

■ ACKNOWLEDGMENTS

Funding from Northeastern University and the National Institutes of Health for the medicinal chemistry

(R01AI082577 to M.P.P.), *T. cruzi* CYP51, and X-ray crystallography (NIH GM067871 to G.I.L.) is gratefully acknowledged. We appreciate a free academic license to the OpenEye suite of software.

■ ABBREVIATIONS USED

HTS, high-throughput screening; CYP51, cytochrome P450 sterol 14 α -demethylase; SAR, structure–activity relationship; *T. cruzi*, *Trypanosoma cruzi*; VNF, (4-(4-chlorophenyl)-*n*-[2-(1*h*-imidazol-1-yl)-1-phenylethyl]benzamide

■ REFERENCES

- (1) World Health Organization. <http://www.who.int/mediacentre/factsheets/fs340/en/index.html>, 2012.
- (2) Pinazo, M. J.; Espinosa, G.; Gállego, M.; López-Chejade, P. L.; Urbina, J. A.; Gascón, J. Successful treatment with posaconazole of a patient with chronic Chagas disease and systemic lupus erythematosus. *Am. J. Trop. Med. Hyg.* **2010**, *82*, 583–587.
- (3) Urbina, J. A.; Payares, G.; Sanoja, C.; Molina, J.; Lira, R.; Brenner, Z.; Romanha, A. J. Parasitological cure of acute and chronic experimental Chagas disease using the long-acting experimental triazole TAK-187. Activity against drug-resistant *Trypanosoma cruzi* strains. *Int. J. Antimicrob. Agents* **2003**, *21*, 39–48.
- (4) Kraus, J. M.; Verlinde, C. L.; Karimi, M.; Lepesheva, G. I.; Gelb, M. H.; Buckner, F. S. Rational modification of a candidate cancer drug for use against Chagas disease. *J. Med. Chem.* **2009**, *52*, 1639–1647.
- (5) Hücke, O.; Gelb, M. H.; Verlinde, C. L.; Buckner, F. S. The protein farnesyltransferase inhibitor Tipifarnib as a new lead for the development of drugs against Chagas disease. *J. Med. Chem.* **2005**, *48*, 5415–5418.
- (6) Buckner, F. In *Drug Targets in Kinetoplastid Parasites*; Majumder, H., Ed.; Springer: New York, 2008; Vol. 625, pp 61–80.
- (7) Urbina, J. A. Ergosterol biosynthesis and drug development for Chagas disease. *Mem. Inst. Oswaldo Cruz* **2009**, *104*, 311–318.
- (8) Andriani, G.; Chessler, A. D.; Courtemanche, G.; Burleigh, B. A.; Rodriguez, A. Activity in vivo of anti-*Trypanosoma cruzi* compounds selected from a high throughput screening. *PLoS Neglected Trop. Dis.* **2011**, *5*, e1298.
- (9) Bettiol, E.; Samanovic, M.; Murkin, A. S.; Raper, J.; Buckner, F.; Rodriguez, A. Identification of three classes of heteroaromatic compounds with activity against intracellular *Trypanosoma cruzi* by chemical library screening. *PLoS Neglected Trop. Dis.* **2009**, *3*, e384.
- (10) Gunatilleke, S. S.; Calvet, C. M.; Johnston, J. B.; Chen, C.-K.; Erenburg, G.; Gut, J.; Engel, J. C.; Ang, K. K. H.; Mulvaney, J.; Chen, S.; Arkin, M. R.; McKerrow, J. H.; Podust, L. M. Diverse inhibitor chemotypes targeting *Trypanosoma cruzi* CYP51. *PLoS Neglected Trop. Dis.* **2012**, *6*, e1736.
- (11) Veber, D. F.; Johnson, S. R.; Cheng, H. Y.; Smith, B. R.; Ward, K. W.; Kopple, K. D. Molecular properties that influence the oral bioavailability of drug candidates. *J. Med. Chem.* **2002**, *45*, 2615–2623.
- (12) Kraus, J. M.; Tatipaka, H. B.; McGuffin, S. A.; Chennamaneni, N. K.; Karimi, M.; Arif, J.; Verlinde, C. L.; Buckner, F. S.; Gelb, M. H. Second generation analogues of the cancer drug clinical candidate tipifarnib for anti-Chagas disease drug discovery. *J. Med. Chem.* **2010**, *53*, 3887–3898.
- (13) Lepesheva, G. I.; Hargrove, T. Y.; Anderson, S.; Kleshchenko, Y.; Furtak, V.; Wawrzak, Z.; Villalta, F.; Waterman, M. R. Structural insights into inhibition of sterol 14 α -demethylase in the human pathogen *Trypanosoma cruzi*. *J. Biol. Chem.* **2010**, *285*, 25582–25590.
- (14) Lepesheva, G. I.; Ott, R. D.; Hargrove, T. Y.; Kleshchenko, Y. Y.; Schuster, I.; Nes, W. D.; Hill, G. C.; Villalta, F.; Waterman, M. R. Sterol 14 α -demethylase as a potential target for antitrypanosomal therapy: enzyme inhibition and parasite cell growth. *Chem. Biol.* **2007**, *14*, 1283–1293.
- (15) Hopkins, A. L.; Groom, C. R.; Alex, A. Ligand efficiency: a useful metric for lead selection. *Drug Discovery Today* **2004**, *9*, 430–431.
- (16) Kalgutkar, A. S.; Dalvie, D.; Obach, R. S.; Smith, D. A. *Reactive Drug Metabolites*; Wiley-VCH Verlag GmbH & Co. KGaA: New York, 2012; pp 93–129.
- (17) Lepesheva, G. I.; Ott, R. D.; Hargrove, T. Y.; Kleshchenko, Y. Y.; Schuster, I.; Nes, W. D.; Hill, G. C.; Villalta, F.; Waterman, M. R. Sterol 14 α -demethylase as a potential target for antitrypanosomal therapy: Enzyme inhibition and parasite cell growth. *Chem. Biol.* **2007**, *14*, 1283–1293.
- (18) Lepesheva, G. I.; Hargrove, T. Y.; Anderson, S.; Kleshchenko, Y.; Furtak, V.; Wawrzak, Z.; Villalta, F.; Waterman, M. R. Structural insights into inhibition of sterol 14 α -demethylase in the human pathogen *Trypanosoma cruzi*. *J. Biol. Chem.* **2010**, *285*, 25582–25590.
- (19) Lepesheva, G. I.; Waterman, M. R. Sterol 14 α -demethylase (CYP51) as a therapeutic target for human trypanosomiasis and leishmaniasis. *Curr. Top. Med. Chem.* **2011**, *11*, 2060–2071.
- (20) Hargrove, T. Y.; Wawrzak, Z.; Liu, J.; Nes, W. D.; Waterman, M. R.; Lepesheva, G. I. Substrate preferences and catalytic parameters determined by structural characteristics of sterol 14 α -demethylase (CYP51) from *Leishmania infantum*. *J. Biol. Chem.* **2011**, *286*, 26838–26848.
- (21) Lepesheva, G. I.; Park, H. W.; Hargrove, T. Y.; Vanhollebeke, B.; Wawrzak, Z.; Harp, J. M.; Sundaramoorthy, M.; Nes, W. D.; Pays, E.; Chaudhuri, M.; Villalta, F.; Waterman, M. R. Crystal structures of *Trypanosoma brucei* sterol 14 α -demethylase and implications for selective treatment of human infections. *J. Biol. Chem.* **2010**, *285*, 1773–1780.
- (22) Buckner, F. S.; Bahia, M. T.; Suryadevara, P. K.; White, K. L.; Shackleford, D. M.; Chennamaneni, N. K.; Hulverson, M. A.; Laydbak, J. U.; Chatelain, E.; Scandale, I.; Verlinde, C. L. M. J.; Charman, S. A.; Lepesheva, G. I.; Gelb, M. H. Pharmacological characterization, structural studies, and in vivo activities of anti-Chagas disease lead compounds derived from tipifarnib. *Antimicrob. Agents Chemother.* **2012**, *56*, 4914–4921.
- (23) Lepesheva, G. I.; Waterman, M. R. Structural basis for conservation in the CYP51 family. *Biochim. Biophys. Acta* **2011**, *1814*, 88–93.
- (24) Buckner, F. S.; Verlinde, C. L.; La Flamme, A. C.; Van Voorhis, W. C. Efficient technique for screening drugs for activity against *Trypanosoma cruzi* using parasites expressing beta-galactosidase. *Antimicrob. Agents Chemother.* **1996**, *40*, 2592–2597.
- (25) Lepesheva, G. I.; Zaitseva, N. G.; Nes, W. D.; Zhou, W.; Arase, M.; Liu, J.; Hill, G. C.; Waterman, M. R. CYP51 from *Trypanosoma cruzi*: a phyla-specific residue in the B' helix defines substrate preferences of sterol 14 α -demethylase. *J. Biol. Chem.* **2006**, *281*, 3577–3585.